Discrete-time causal control of WECs with finite stroke, in stochastic waves

Jeffrey T Scruggs, Yejun Lao, Mirko Previsic, and Anantha Karthikeyan

***Abstract*—We consider the problem of feedback control design for wave energy converters in which the power take-off system has a finite stroke limit. In particular, we consider the situation in which the waves are modeled as a stationary stochastic process with known spectrum, and the wave energy converter dynamics can be approximated as linear. For this scenario, we develop a technique for the design of a discrete-time feedback controller for the power take-off system. The design technique has three stages. In the first stage, a linear feedback controller is optimized for stationary power generation, while imposing a relaxed version of the maximum stroke constraint on the design. In the second stage, a supplemental nonlinear feedback loop is proposed, for the purpose of stroke protection. In the third stage, the two designs (linear and nonlinear) are fused in a manner that preserves stability of the overall system. The design technique is demonstrated on a simulation of a simple cylindrical buoy. We further show, through this example, that the nonlinear controller may be tuned through the adjustment of a scalar parameter, which adjusts the trade-off between mean generated power, and the force levels required to protect the stroke.**

***Index Terms*—Control, Discrete-time, Stochastic waves, Stroke saturation**

I. Introduction

Wave energy converter (WEC) technologies have been the subject of considerable research and development for over half a century [1]–[10]. The array of concepts that have been proposed is vast and diverse, and defies the use of generalities. Nonetheless, many of the more successful technologies can be characterized by a mechanical structure comprised of multiple degrees of freedom, which responds dynamically in the waves. In such systems, the power take-off (PTO) system is embedded within this dynamically-excited structure between two of its degrees of freedom, and extracts power - either by hydraulic or electromechanical means - by regulating the force it applies between these degrees of freedom. In many cases, the PTO hardware has only a finite distance over which it may extend and contract, which we call a *stroke limit* [11]–[15]. In such situations, the presence of this stroke limit results in a constraint on the relative displacements of the two degrees of freedom to which the PTO is attached. If the PTO is not explicitly controlled to stay within these limits, collisions occur which we refer to as *stroke saturation*.

Stroke saturation is undesirable for a few reasons. Most importantly, it imposes impulsive loads on the PTO hardware as well as the surrounding structure, potentially resulting in damage or fatigue. Beyond the prospect of damage, these dynamic effects can alter the response of the WEC system in such a way as to be detrimental to overall power generation performance. This is especially true for situations in which the PTO is actively controlled for maximal power generation, and endowed with the ability to both absorb and inject power. In such situations, the presence of unmodeled stroke saturation can destabilize an otherwise-optimally controlled WEC.

In this paper we consider the design of controllers for WECs with finite stroke, when subjected to stochastic waves. In particular we consider causal control algorithms; i.e., control laws that do not require future wave loads to be known a priori (e.g., through preview sensors) in order to make decisions. (Note that this notion of causality does not, however, preclude the control algorithm from making *predictions* about future behavior based on past and present information.) In the absence of stroke limits on the WEC PTO hardware, and when linear response can be assumed, optimal causal control design for this class of problems is straight-forward. Specifically, it constitutes a special case of Linear Quadratic Gaussian (LQG) control, which may be solved in closed form in terms of a WEC's state space dynamic model [16]. However, the presence of stroke limits complicates the control design significantly, when stochastic waves are assumed. A further challenge in the control design problem arises, when it is necessary to implement causal control algorithms in discrete-time.

We present a technique for discrete-time control of WECs with finite stroke, which is based on multi-objective optimal control, as well as passivity theory. The design technique is comprised of several components which can be designed in sequence. First, an optimal linear LQG controller is designed which accommodates a weakened, time-averaged version of the stroke limit constraint. This first design component makes use of multi-objective optimal control theory, and is cast in the context of a semidefinite program. Second, this controller is nested inside a nonlinear passive feedback law that protects the stroke from saturation. This stage makes use of nonlinear passivity theory. Third, the two components are integrated together in a very specific way which guarantees mean-square stability in stationary response. In prior work (i.e.,

Manuscript ID: 1705 Conference Track: Grid integration, power take-off and control. This material is based upon work supported by the Department of Energy, Office of Energy Efficiency and Renewable Energy (EERE), under Award Number DE-EE0007173.

Jeff Scruggs and Yejun Lao are with the Department of Civil and Environmental Engineering, University of Michigan, Ann Arbor, MI, USA. (e-mail: jscruggs@umich.edu, waynelao@umich.edu)

Mirko Previsic and Anantha Karthikeyan are with ReVision Consulting, LLC, Sacramento, CA, USA. (e-mail: mirko@re-vision.net, anantha@re-vision.net)

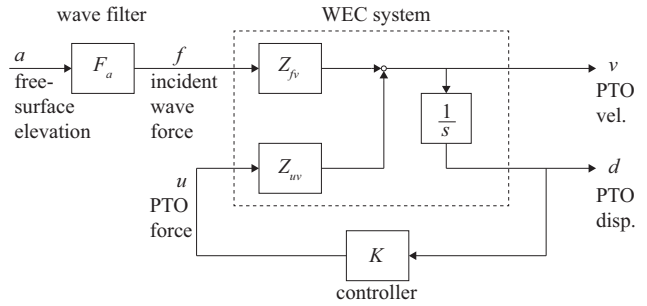

Fig. 1. Block diagram of linear dynamic model for controlled WEC

[17], [18]), the authors have presented a variant of this general technique which is applicable to continuous-time systems. In the present paper, the technique is developed explicitly for control algorithms that must be implemented in discrete-time; a restriction which introduces an added layer of complexity.

The paper is organized as follows. Section II details the manner in which we model a WEC for the purposes of discrete-time control for optimal power generation. Section III illustrates the first step in the control design methodology, involving the optimization of a linear control law. Section IV illustrates the second and third steps, involving nonlinear passivity-based control. Finally, Section V contains a simulation example that illustrates the main features of the methodology on a simple heaving buoy point absorber model.

II. Dynamic modeling

A. Continuous-time dynamic model

With reference to Figure 1, let $d(t)$ be the displacement of the PTO, and $v(t) = \frac{d}{dt}d(t)$ be the corresponding extension velocity. Let $u(t)$ be the corresponding PTO force. For this analysis we presume $u(t)$ can be controlled with high-bandwidth by the WEC control system, and therefore consider it to be the control input to the system. Let $f(t)$ be the vector of forces on the various degrees of freedom of the WEC due to the propagation of incident waves, characterized by the free-surface elevation $a(t)$ at a fixed location relative to the WEC. Then in the frequency domain we have that

$$\hat{v}(j\omega) = Z_{fv}(j\omega)\hat{f}(j\omega) + Z_{uv}(j\omega)\hat{u}(j\omega) \tag{1}$$

where $Z_{fv}(s)$ and $Z_{uv}(s)$ are causal transfer functions characterizing the linear WEC dynamics, and where the "hat" accent denotes the Fourier transform. These linear transfer functions are obtained from a hydrodynamic analysis of the WEC, either via the use of analytical solutions to the hydrodynamic coefficients (for simple WEC geometries) or via numerical analysis [6].

We assume the free surface elevation to be a stochastic process with power spectral density $S_a(\omega)$, with the convention that the autocorrelation of the free-surface elevation is related to $S_a(\omega)$ via the inverse Fourier transform; i.e.,

$$\mathcal{E}a(t)a(t+\tau) = \frac{1}{2\pi}\int_{-\infty}^{\infty} e^{j\omega\tau} S_a(\omega)d\omega \tag{2}$$

We further assume that the free surface elevation produces wave force f in the frequency domain via

$$\hat{f}(j\omega) = F_a(j\omega)\hat{a}(j\omega) \tag{3}$$

where $F_a(j\omega)$ is the (non-causal) linear transfer function characterizing the linear hydrodynamic excitation. It follows from these assumptions that the incident wave force may be viewed as a stochastic process with power spectral density

$$S_f(j\omega) = F_a(j\omega)S_a(\omega)F_a^T(-j\omega) \tag{4}$$

We note that the above result is unaffected by the non-causality of $F_a(j\omega)$.

Regarding the continuous-time model, we make three additional assumptions which must be true in order for the model to be consistent with physical insight.

1) Firstly, we require that $Z_{uv}(s)$ be positive-real; i.e., we require that it be analytic in the open right-half plane, with the condition
$$Z_{uv}(\sigma + j\omega) + Z_{uv}^T(\sigma - j\omega) \geqslant 0 \tag{5}$$
for all $\sigma > 0$. This condition is true if and only if the mapping $u \mapsto v$ is passive [19], which is imposed by the thermodynamics of the WEC system.
2) Secondly, we require that $Z_{uv}(s)$ have bounded gain; i.e., we require that
$$\sup_{\omega\in\mathbb{R}} \|Z_{uv}(j\omega)\| < \infty \tag{6}$$
Loosely speaking, this is equivalent to requiring that the WEC system must be such that the mapping $u \mapsto v$ has bounded gain at resonance, contains no rigid body modes, and contains no ideal derivatives.
3) Thirdly, we assume that the mappings $u \mapsto d$ and $f \mapsto d$ have bounded gain in the frequency domain. Recognizing that $d(t)$ is the integral of $v(t)$, this is equivalent to requiring that
$$\sup_{\omega\in\mathbb{R}} \left\| \tfrac{1}{j\omega} Z_{uv}(j\omega) \right\| < \infty \tag{7}$$
$$\sup_{\omega\in\mathbb{R}} \left\| \tfrac{1}{j\omega} Z_{fv}(j\omega) \right\| < \infty \tag{8}$$
Loosely speaking, this is equivalent to requiring that the response of the WEC PTO displacement remains bounded in open-loop, for all bounded inputs.

In the sequel, we will refer to the above three assumptions as A1, A2, and A3.

B. Discrete-time dynamic model

We assume that $u(t)$ is controlled in discrete-time, via a zero-order-hold convention; i.e.,

$$u(t) = u_k, \quad t \in [kT, (k+1)T) \tag{9}$$

where T is the sample time and k is the discrete time index. We similarly refer to other output signals sampled at time $t = kT$ with a subscript k; i.e., $v_k = v(kT)$, $d_k = d(kT)$, etc.

We assume that the dissipation in the power train of the WEC can be adequately modeled as a quadratic function of the PTO force; i.e.,

$$p_{diss}(t) = u^T(t)C^{-1}u(t) \tag{10}$$

where C is a matrix with units of viscous damping. Let p_k be the average power generation over interval $t \in [kT, (k+1)T)$. Then due to the zero-order-hold convention, we have that

$$\begin{aligned} p_k =& \tfrac{1}{T}\int_{kT}^{(k+1)T} \left[-u^T(t)v(t) - p_{diss}(t)\right] dt && (11)\\ =& -\tfrac{1}{T}u_k^T C^{-1}u_k - u_k^T\tfrac{1}{T}\int_{kT}^{(k+1)T} v(t)dt && (12)\\ =& -u_k^T R u_k - u_k^T\tfrac{1}{T}\left(d_{k+1} - d_k\right) && (13)\end{aligned}$$

where $R \triangleq C^{-1}$. Letting

$$q_k \triangleq \tfrac{1}{T}\left(d_{k+1} - d_k\right), \tag{14}$$

we have that

$$p_k = -u_k^T R u_k - u_k^T q_k \tag{15}$$

Let the z-transforms of the discrete-time sampled variables be denoted by overbars; i.e., for discrete-time signal q_k,

$$\bar{q}(z) = \sum_{k=-\infty}^{\infty} z^{-k} q_k \tag{16}$$

Then following the methodology outlined in [20], the linear dynamics of the WEC as described above are equivalent to the discrete time system

$$\bar{q}(z) = H_{wq}(z)\bar{w}(z) + H_{uq}(z)\bar{u}(z) \tag{17}$$

where $\{w_k, k \in \mathbb{Z}\}$ is an independent, identically distributed Gaussian stochastic sequence with $\mathcal{E}w_k = 0$ and $\mathcal{E}w_k w_k^T = I$. Transfer function $H_{uq}(z)$ is solved in the frequency domain (i.e., for $z = e^{j\Omega},\ \Omega \in [-\pi, \pi]$) via

$$H_{uq}(e^{j\Omega}) = \sum_{\ell=-\infty}^{\infty} Z_{uv}(j\omega)\,\mathrm{sn}\left(\omega T/2\right)^2\Big|_{\omega=\Omega/T+2\pi\ell/T} \tag{18}$$

with the transfer function $H_{uq}(z)$ obtained from the frequency-domain solution as the analytic continuation for all $|z| > 1$. Meanwhile, transfer function $H_{wq}(z)$ is found by first finding the discrete-time power spectral density

$$\begin{aligned}\Sigma_{wq}(j\Omega) = \sum_{\ell=-\infty}^{\infty} &\frac{1}{T} Z_{fv}(j\omega) S_f(j\omega)\\ &\times Z_{fv}^T(-j\omega)\,\mathrm{sn}(\omega T/2)^2\big|_{\omega=\Omega/T+2\pi\ell/T}\end{aligned} \tag{19}$$

Then, from Σ_{wq}, transfer function $H_{wq}(z)$ is its unique minimum-phase spectral factorization, found as the solution to

$$\Sigma_{wq}(j\Omega) = H_{wq}(e^{j\Omega})H_{wq}(e^{-j\Omega})^T \tag{20}$$

We note that for the discrete-time system model, three respective properties are inherited from Assumptions A1, A2, and A3:

1) $H_{uq}(z)$ is positive-real in discrete-time; i.e., it is analytic in the open region of the complex plane exterior to the unit disk, and
$$H_{uq}(\beta e^{j\Omega}) + H_{uq}(\beta e^{-j\Omega})^T \geqslant 0 \tag{21}$$
for all $\beta \in \mathbb{R}$ with $|\beta| > 1$.
2) $H_{uq}(z)$ has bounded gain; i.e.,
$$\sup_{\Omega\in[-\pi,\pi]} \|H_{uq}(e^{j\Omega})\| < \infty \tag{22}$$
3) $H_{uq}(z)$ and $H_{wq}(z)$ have zeros at the $z = 1$; i.e.,
$$\lim_{z\to 1} H_{uq}(z) = 0 \tag{23}$$
$$\lim_{z\to 1} H_{wq}(z) = 0 \tag{24}$$

C. Finite-dimensional discrete-time model

We assume that H_{uq} and H_{wq} have been approximated as finite-dimensional linear discrete-time systems, using a system identification technique. For example, in [16] subspace techniques are used to identify H_{uq}. In [20], H_{wq} is identified using the subspace spectral factorization technique described in [21]. The same procedures are used in the present paper, resulting in the discrete-time model we shall use for the remainder of the paper:

$$\begin{aligned} x_{k+1} =& Ax_k + B_w w_k + B_u u_k && (25)\\ q_k =& C_q x_k + D_{wq} w_k + D_{uq} u_k && (26)\end{aligned}$$

We assume that the identified realization is minimal; i.e., that all uncontrollable or unobservable modes have been eliminated.

We assume that in approximating the system via a finite dimensional state space, the identification of the model parameters has been constrained such that the properties inherited from Assumptions A1, A2, and A3 still hold for finite-dimensional approximations

$$H_{uq}(z) \approx C_q[zI - A]^{-1}B_q + D_{uq} \tag{27}$$
$$H_{wq}(z) \approx C_q[zI - A]^{-1}B_w + D_{wq} \tag{28}$$

In terms of the finite-dimensional state space parameters, this implies the following properties:

1) *Theorem 1:* **[?]** Let $C_q[zI - A]^{-1}B_q + D_{uq}$ be positive-real and define $\tilde{R} \triangleq R + \frac{1}{2}D_{uq} + \frac{1}{2}D_{uq}^T$. Then if $\tilde{R} > 0$ then the Riccati equation
$$W = A^T W A + F^T\left(\tilde{R} - B_u^T W B_u\right)F \tag{29}$$
with
$$F \triangleq -\left(\tilde{R} - B_u^T W B_u\right)^{-1}\left(\tfrac{1}{2}C_q^T - A^T W B_u\right)^T \tag{30}$$
has a unique solution for which the matrix $A + B_u F$ is asymptotically stable.
2) Matrix A is asymptotically stable in discrete time; i.e., its eigenvalues lie exclusively within the open unit disk in the complex plane.
3) $H_{uq}(z)$ and $H_{wq}(z)$ have zeros at the origin, implying that
$$D_{uq} + C_q\left[I - A\right]^{-1}B_u = 0 \tag{31}$$
$$D_{wq} + C_q\left[I - A\right]^{-1}B_w = 0 \tag{32}$$

Note that for this model, it is the case that

$$d_{k+1} = d_0 + T\sum_{i=0}^{k} q_i \tag{33}$$

$$= d_0 + T\sum_{i=0}^{k} C_q x_i + D_w w_i + D_q u_i \tag{34}$$

which, using the consequence of assumption A3 above, implies

$$d_{k+1} = d_0 + TC_q[I-A]^{-1}\sum_{i=0}^{k}(x_i - Ax_i - B_w w_i - B_u u_i) \tag{35}$$

$$= d_0 + TC_q[I-A]^{-1}\sum_{i=0}^{k}(x_i - x_{i+1}) \tag{36}$$

$$= d_0 + TC_q[I-A]^{-1}x_0 - TC_q[I-A]^{-1}x_{k+1} \tag{37}$$

Assuming the system is initiated at a zero initial state at $k=0$, then it follows that

$$d_k = C_d x_k \tag{38}$$

where $C_d \triangleq -TC_q[I-A]^{-1}$.

III. Optimal linear control design with mean-square stroke constraints

We wish to design a feedback law $\mathcal{K}: d \mapsto u$ which maximizes the mean power generation $\bar{p} \triangleq \mathcal{E}p$, with the expectation evaluated in stationary response. In this section we begin with the design of a linear controller, which while not explicitly enforcing the stroke constraints at every time, enforces them in a mean-square sense. In the next section we will then design a nonlinear controller, based on this linear design, which does enforce the stroke constraints at every time, explicitly.

To be more specific, suppose that the true stroke limit of the PTO is d_m; i.e., the condition $|d(t)| \leqslant d_m$ must be enforced. In order to enforce this explicitly, nonlinear control is required. In this section, we replace this condition with a more relaxed one, which places a constraint on the mean-square value of the stroke; i.e., on the quantity

$$s_d \triangleq \mathcal{E}d^2 \tag{39}$$

with the expectation taken in stationarity.

Specifically, our constraint will be of the form

$$s_d \leqslant \tfrac{1}{4}d_m^2 \tag{40}$$

To see why this specific condition is to be imposed, consider the distribution on the peaks of $d(t)$. For narrow to moderate band processes, this distribution for a particular peak ψ can be approximated as a Rayleigh distribution, with cumulative distribution function

$$P[\psi \leqslant \psi_0] = 1 - \exp\left\{-\psi_0^2/2s_d\right\} \tag{41}$$

As such, constraining s_d as in (39) ensures that the probability of a given peak being in violation of the stroke constraint for the linear controller is approximately $e^{-2} \approx 0.14$. As such, it ensures that the linear controller will render most peaks within the stroke limit, with only the outliers needing to be dealt with via nonlinear control.

For the linear control design, we consider finite-dimensional time-invariant controllers, which can be parametrized by matrices $\{A_K, B_K, C_K\}$ in the feedback form

$$\xi_{k+1} = A_K\xi_k + B_K d_k \tag{42}$$

$$u_k = C_K\xi_k \tag{43}$$

This results in an augmented closed-loop system

$$\chi_{k+1} = A_{cl}\chi_k + B_{wcl}w_k \tag{44}$$

$$q_k = C_{qcl}\chi_k + D_{qcl}w_k \tag{45}$$

$$d_k = C_{dcl}\chi_k \tag{46}$$

$$u_k = C_{ucl}\chi_k \tag{47}$$

where

$$A_{cl} = \begin{bmatrix} A & B_uC_K \\ B_KC_d & A_K \end{bmatrix} \tag{48}$$

$$B_{wcl} = \begin{bmatrix} B_w \\ 0 \end{bmatrix} \tag{49}$$

$$C_{qcl} = \begin{bmatrix} C_q & D_{uq}C_K \end{bmatrix} \tag{50}$$

$$D_{qcl} = D_{wq} \tag{51}$$

$$C_{dcl} = \begin{bmatrix} C_d & 0 \end{bmatrix} \tag{52}$$

$$C_{ucl} = \begin{bmatrix} 0 & C_K \end{bmatrix} \tag{53}$$

We then consider the following optimization problem:

$$\begin{array}{ll} \text{Given:} & A, B_w, B_u, C_q, D_{wq}, D_{uq}, C_d \\ \text{Maximize:} & \bar{p} \triangleq \mathcal{E}p \\ \text{Constraint:} & s_d < \frac{1}{4}d_m^2 \\ \text{Over:} & A_K, B_K, C_K \end{array} \tag{54}$$

where in the above problem, the expectations are taken in stationarity.

To perform this optimization, we need the following theorem:

Theorem 2: [22] For any linear feedback parameters $\{A_K, B_K, C_K\}$ which stabilize the closed-loop system,

$$\bar{p} = \bar{p}_0 - \mathcal{E}\left\{(u-Fx)^T\,\Delta\,(u-Fx)\right\} \tag{55}$$

where F is as in (30),

$$p_0 \triangleq \operatorname{tr}\{B_w^T W B_w\} \tag{56}$$

and $\Delta \triangleq \tilde{R} - B_u^T W B_u$.

Using the above theorem, it follows that the maximization of average generated power is equivalent to the minimization of the second term on the right-hand side of (55), which is positive semidefinite. In particular, it leads to the following result:

Theorem 3: Control parameters $\{A_K, B_K, C_K\}$ result in the mean power generation bound $\bar{p} > \gamma$ and mean-square stroke bound $s_d < \frac{1}{4}d_m^2$, for some $\gamma \in \mathbb{R}$, if and only if there exists a matrix $S = S^T > 0$ such that

$$S - A_{cl}SA_{cl}^T - B_{wcl}B_{wcl}^T > 0 \tag{57}$$

$$(F_{cl} - C_{ucl})\,S\,(F_{cl} - C_{ucl})^T < \bar{p}_0 - \gamma \tag{58}$$

$$C_{dcl}SC_{dcl}^T < \tfrac{1}{4}d_m^2 \tag{59}$$

where $F_{cl} \triangleq \begin{bmatrix} F & 0 \end{bmatrix}$.

Proof: Let $\Sigma = \mathcal{E}\chi\chi^T$. Then Σ is the solution to Lyapunov equation

$$A_{cl}\Sigma A_{cl}^T - \Sigma + B_{wcl}B_{wcl}^T = 0 \tag{60}$$

and the existence of closed-loop stationarity implies that $\Sigma \geqslant 0$ and that A_{cl} is asymptotically stable in discrete-time. The corresponding power generation performance is then as in (55), i.e.,

$$\bar{p} = \bar{p}_0 - (F_{cl} - C_{ucl})\,\Sigma\,(F_{cl} - C_{ucl})^T \tag{61}$$

Now, let S be the solution to

$$A_{cl}SA_{cl}^T - S + B_{wcl}B_{wcl}^T = -\epsilon I \tag{62}$$

for some $\epsilon > 0$. It follows that

$$A_{cl}(S-\Sigma)A_{cl}^T - (S-\Sigma) = -\epsilon I \tag{63}$$

which, due to the asymptotic stability of A_{cl} implies that $S - \Sigma > 0$. As a result, we have that

$$\gamma \triangleq \bar{p}_0 - (F_{cl} - C_{ucl})\,S\,(F_{cl} - C_{ucl})^T \tag{64}$$

$$= \bar{p} - \delta \tag{65}$$

where

$$\delta = (F_{cl} - C_{ucl})\,(S-\Sigma)\,(F_{cl} - C_{ucl})^T \tag{66}$$

By making ϵ arbitrarily small, δ can be made arbitrarily small and consequently γ can be made to approach $\bar{p}$ from below. A similar argument can be made for the constraint on s_d, and noting that

$$s_d = C_{dcl}\Sigma C_{dcl}^T \tag{67}$$

This proves necessity.

To prove sufficiency, we note that if $S = S^T > 0$ satisfies (57) then A_{cl} must be asymptotically stable, implying the existence of a stationary solution to $\Sigma = \mathcal{E}\chi\chi^T > 0$ satisfying (60). We then have that $S - \Sigma$ satisfies

$$A_{cl}(S-\Sigma)A_{cl}^T - (S-\Sigma) < 0 \tag{68}$$

which, due to the asymptotic stability of A_{cl} implies that $S - \Sigma > 0$. This guarantees that $\delta > 0$ and thus that $\bar{p} < \gamma$. It similarly guarantees that $C_{dcl}(S-\Sigma)C_{dcl}^T > 0$, and consequently that $\frac{1}{4}d_m^2 > s_d$. ■

This theorem is useful because it leads to a convex characterization of the problem, as shown below. That this result follows from Theorem 3 is a direct result of methodologies put forth in [23], and consequently in the interest of brevity we omit the proof here.

Theorem 4: There exists a set of control parameters $\{A_K, B_K, C_K\}$ resulting in mean power generation bound $\bar{p} > \gamma$ and mean-square stroke bound $s_d < \frac{1}{4}d_m^2$, for some $\gamma \in \mathbb{R}$, if and only if there exist matrices $X = X^T > 0$, $Y = Y^T > 0$ $\hat{A}$, $\hat{B}$, and $\hat{C}$ such that

$$\begin{bmatrix} X & I & AX + B_u\hat{C} \\ I & Y & \hat{A} \\ XA^T + \hat{C}^TB_u^T & \hat{A}^T & X \\ A^T & A^TY + C_d^T\hat{B}^T & I \\ B_w^T & B_w^TY & 0 \end{bmatrix} \begin{bmatrix} A & B_w \\ YA + \hat{B}C_d & YB_w \\ I & 0 \\ Y & 0 \\ 0 & I \end{bmatrix} > 0 \tag{69}$$

$$\begin{bmatrix} p_0 - \gamma & FX - \hat{C} & F \\ XF^T - \hat{C}^T & X & I \\ F^T & I & Y \end{bmatrix} > 0 \tag{70}$$

$$\begin{bmatrix} \frac{1}{4}d_m^2 & C_dX & C_d \\ XC_d^T & X & I \\ C_d^T & I & Y \end{bmatrix} > 0 \tag{71}$$

One such controller can be found as

$$A_K = N^{-1}\left(\hat{A} - \hat{B}C_dX - YB_u\hat{C} - YAX\right)M^{-T} \tag{72}$$

$$B_K = N^{-1}\hat{B} \tag{73}$$

$$C_K = \hat{C}M^{-T} \tag{74}$$

where M and N are any matrices such that $MN^T = I - XY$.

The above theorem provides a convex domain over which to optimize a linear controller. Specifically, the optimal control problem from (54) becomes, equivalently,

$$\begin{array}{ll} \text{Given:} & A, B_w, B_u, C_q, D_{wq}, D_{uq}, C_d, d_m \\ \text{Maximize:} & \gamma \\ \text{Constraints:} & (69), (70), (71) \\ \text{Over:} & X = X^T, Y = Y^T, \hat{A}, \hat{B}, \hat{C}, \gamma \end{array} \tag{75}$$

IV. Nonlinear stroke protection loop

Consider the feedback architecture as shown in Figure 2, in which the linear controller $\mathcal{K}$ optimized in the previous section is augmented with nonlinear feedback. The consequence of this is a total PTO force at time k which is a summation of the linear and nonlinear parts; i.e.,

$$u_k = u_k^\ell + u_k^n \tag{76}$$

where the linear control force u_k^ℓ is designed as in the previous section; i.e.,

$$u_k^\ell = C_K\xi_k \tag{77}$$

We may therefore view the nonlinear control loop as introducing a supplemental restoring force u_k^n which modifies the optimized linear feedback, when necessary, to prevent stroke saturation.

As shown, this nonlinear control loop consists of two components. The first of these is a one-step-ahead predictor, which forecasts the displacement that will result at discrete time $k+1$ (i.e., d_{k+1}) assuming only the linear control force is applied; i.e., assuming $u_k = u_k^\ell$. This forecast is made using the values of y and u up to

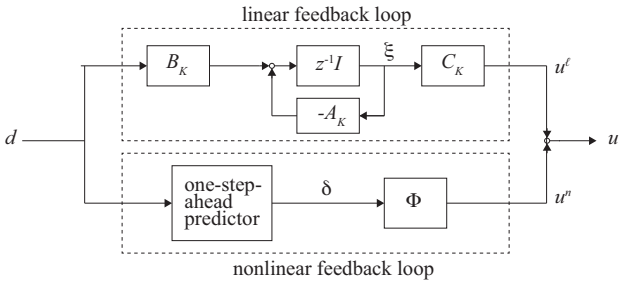

Fig. 2. Block diagram of linear and nonlinear control loops

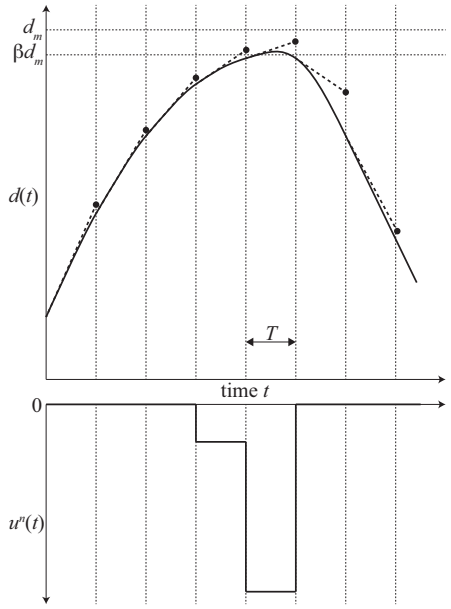

Fig. 3. Upper plot: Trajectory for d (solid) with one-step-ahead prediction trajectories (dashed). Lower plot: Corresponding trajectory for nonlinear force u^n

and including discrete-time k. We denote this forecast as δ_k.

The second part of the nonlinear control loop is the nonlinear function $u_k^n = \Phi(\delta_k)$, which acts as a kind of discrete-time "hard spring," producing a significant decelerative force when necessary. To illustrate the qualitative manner in which this is done, consider Figure 3, which shows a hypothetical time history for several discrete time steps over which d_k approaches its maximum allowable stroke d_m. As shown, the one-step-ahead predictor produces a forecast, at time k, of where d_{k+1} will be if u_k^n is made equal to 0. When this forecast has a magnitude well below d_m, the PTO stroke is deemed to be within its "safe zone" and $u_k^n = 0$. However, when the forecast has a magnitude above some threshold βd_m, for $\beta < 1$ equal to some safety factor (say, 0.9), the PTO stroke is deemed to be exiting its safe zone, triggering the nonlinear control loop to issue a corrective force to reverse its direction.

A. One-step-ahead predictor design

First note that

$$d_{k+1} = d_k + Tq_k \tag{78}$$
$$= d_k + T\left(C_q x_k + D_{uq}u_k + D_{wq}w_k\right) \tag{79}$$

We assume that at time k, the information that is known to the controller is comprised of

$$\mathcal{I}_k = \{d_k, u_k, d_{k-1}, u_{k-1}, d_{k-2}, u_{k-2}, ...\} \tag{80}$$

Let the conditional expectation for x_k, given this information, be denoted $\hat{x}_k$; i.e.,

$$\hat{x}_k \triangleq \mathcal{E}\left\{x_k|\mathcal{I}_k\right\} \tag{81}$$

Then it is a fact that $\hat{x}_k$ is found recursively in time via the Kalman filter; i.e.,

$$\hat{x}_{k+1} = \left[A + LC_q\right]\hat{x}_k - Lq_k + B_u u_k \tag{82}$$

where the Kalman gain L is

$$L = -ASC_q^T\left[C_q S C_q^T + D_{wq}D_{wq}^T\right]^{-1} \tag{83}$$

and where the matrix $S = S^T$ is the solution to discrete-time Riccati equation

$$S = ASA^T + B_w B_w^T - ASC_q^T\left[C_q S C_q^T + D_{wq}D_{wq}^T\right]^{-1} C_q S A^T \tag{84}$$

We therefore have that

$$\mathcal{E}\left\{d_{k+1}|\mathcal{I}_k\right\} = d_k + T\left(C_q\hat{x}_k + D_{uq}u_k\right) \tag{85}$$

The forecasted displacement δ_k is the expected value of d_{k+1} for the specific case where the control input u_k is chosen as the linear control input only; i.e., $u_k = C_K\xi_k$, so

$$\delta_k = d_k + T\left(C_q\hat{x}_k + D_{uq}C_K\xi_k\right) \tag{86}$$

Consequently, the expectation of the true displacement and the forecast can be related via

$$\mathcal{E}\left\{d_{k+1}|\mathcal{I}_k\right\} = \delta_k + TD_{uq}u_k^n \tag{87}$$

B. Nonlinearity design

The nonlinear function $\Phi(\cdot)$ is designed to bring about a direction reversal of the one-step-ahead forecast δ_k, such that it remains inside the safe zone. To do this we note that if $\Phi(\delta_k) \neq 0$ then this implies that $|\delta_k| > \beta d_m$. We seek the nonlinear control force u_k^n which will result in

$$\left|\mathcal{E}\left\{d_{k+1}|\mathcal{I}_k\right\}\right| = \beta d_m \tag{88}$$

In other words, we require that

$$\delta_k + TD_{uq}u_k^n = \beta d_m \operatorname{sgn}(\delta_k) \tag{89}$$

resulting in the nonlinear feedback law $\Phi(\cdot)$ as

$$\Phi(\delta_k) = \begin{cases} 0 & : \quad |\delta_k| < \beta d_m \\ \Gamma\left(\beta d_m - |\delta_k|\right)\operatorname{sgn}(\delta_k) & : \quad |\delta_k| \geqslant \beta d_m \end{cases} \tag{90}$$

where

$$\Gamma = \frac{1}{TD_{uq}} \tag{91}$$

C. Stabilization

The nonlinear control loop shown in Figure 2 has the advantage of being heuristic and therefore straightforward to conceptualize, but in general it cannot be implemented without modification. This is because in many situations (including the example in this paper) the nonlinear feedback loop interacts with the linear controller in such a way as to destabilize the closed-loop system. In order to implement the technique, stability must be recovered.

To do this, we first note that the nature of the feedback function $\Phi(\cdot)$, as formulated here, has the special property of passivity, as illustrated in the lemma below. The proof of this lemma is lengthy, and consequently is omitted here in the interest of brevity.

Lemma 1: The feedback function $\Phi(\delta_k)$ in (90) has the property that it is mean-square passive with respect to the q; i.e., for all $N \geqslant 0$, and with $d_0 = 0$, there exists a constant β such that

$$\mathcal{E}\left\{\frac{1}{N}\sum_{k=0}^{N}\Phi(\delta_k)q_k\right\} \leqslant \beta \tag{92}$$

for any Γ in the range

$$\Gamma \in \left[0, \frac{1}{TD_{uq}}\right] \tag{93}$$

The above lemma is important because of the following theorem, which is a standard result from robust control. Its proof can be found in numerous standard references (e.g., [24]) and consequently will be omitted here in the interest of brevity.

Theorem 5: If u_k^n is mean-square passive with respect to q_k, and if the transfer function $u_k^n \mapsto q$ is positive real, then the closed loop interconnection of the two mappings is stable.

From the above theorem, we conclude that if the control architecture from Figure 2 is modified such that $u^n \mapsto q$ is positive real, then closed-loop stability is assured. This can be facilitated by the inclusion of an extra signal path which feeds u_k^n back into the linear control loop, as shown in Figure 4. As shown, this new control architecture involves the design of an additional input matrix B_n which must be designed to bring about positive-realness of the mapping $u^n \mapsto q$; i.e., of the transfer function

$$G_{nq}(z) = C_{qcl}\left[zI - A_{cl}\right]^{-1}\begin{bmatrix}B_u\\B_n\end{bmatrix} + D_{uq} \tag{94}$$

In other words, we require that for all $\Omega \in [-\pi, \pi]$,

$$G_{nq}(e^{j\Omega}) + G_{nq}^T(e^{-j\Omega}) \geqslant 0 \tag{95}$$

By the Positive-real Lemma (shown below), this condition may be made equivalent to an algebraic condition on B_n.

Lemma 2: [25] Condition (95) is true if and only if there exists a matrix $S = S^T > 0$ such that

$$\begin{bmatrix} A_{cl}SA_{cl}^T - S & A_{cl}SC_{qcl}^T - \begin{bmatrix}B_u\\B_n\end{bmatrix} \\ C_{qcl}^TSA_{cl}^T - \begin{bmatrix}B_u\\B_n\end{bmatrix}^T & C_{qcl}SC_{qcl}^T - D_{uq} - D_{uq}^T \end{bmatrix} \leqslant 0 \tag{96}$$

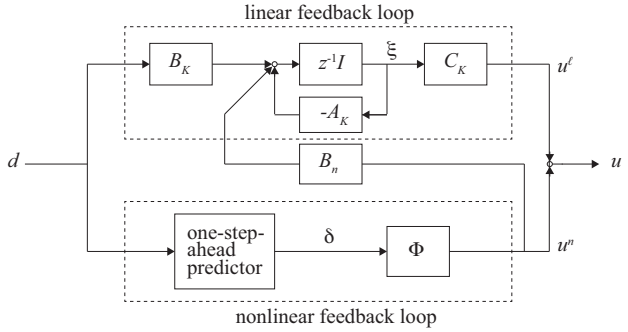

Fig. 4. Block diagram of linear and nonlinear control loops, with coupling matrix B_n

Lemma 2 is important because it gives us a constrained domain over which to optimize B_n. However, it is somewhat unclear how to best determine which B_n, out of all those satisfying (96), is the "optimal" one. In other related studies, the authors have chosen the B_n which optimized the first nonzero Markov parameter for the closed loop system [17], as well as choosing the B_n that minimizes the degree to which u^n excites the linear controller states [18]. However, in the present application it was found that a simpler technique performed at least as well, consisting of the following optimization:

$$\begin{array}{ll} \text{Given:} & A_{cl}, B_u, C_{qcl}, D_{uq} \\ \text{Maximize:} & C_{qcl}SC_{qcl}^T \\ \text{Constraints:} & (96), S > 0 \\ \text{Over:} & S = S^T, B_n \end{array} \tag{97}$$

D. Generalizing the nonlinearity

The formulation of nonlinear feedback law $\Phi(\cdot)$, as in (90), has the advantage of being heuristic. It is reasonably straight-forward to understand how the feedback law makes use of a one-step-ahead forecast in order to facilitate stroke protection. However, there are certain advantages to generalizing the nonlinear feedback law beyond that shown in (90).

Specifically, it is straight-forward to show that all the results on stability in Section IV-C still hold if $\Phi(\cdot)$ is generalized by still implementing equation (90), but redefining δ_k from (86), to

$$\delta_k = d_k + (T+\tau)\left(C_q\hat{x}_k + D_{uq}C_K\xi_k\right) \tag{98}$$

where $\tau > 0$ can be chosen as any nonnegative value. Indeed, this makes the stroke protection algorithm more cautious. More importantly, though, raising the value of τ reduces the magnitude of the nonlinear forces u_k^n. As we shall see in the example in the next section, this comes at the expense of lower power generation with higher τ.

With δ_k redefined as in (98), the value of Γ in (90) must also be changed to assure stability. In this case, (90) is guaranteed to be passive with respect to q, for Γ in the range

$$\Gamma \in \left[0, \frac{1}{D_{uq}(T+\tau)}\right] \tag{99}$$

Although the value in (91) at the upper end of this range works very effectively in theory, in practice the

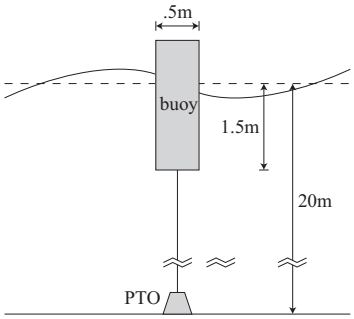

Fig. 5. Buoy-type WEC considered in the example

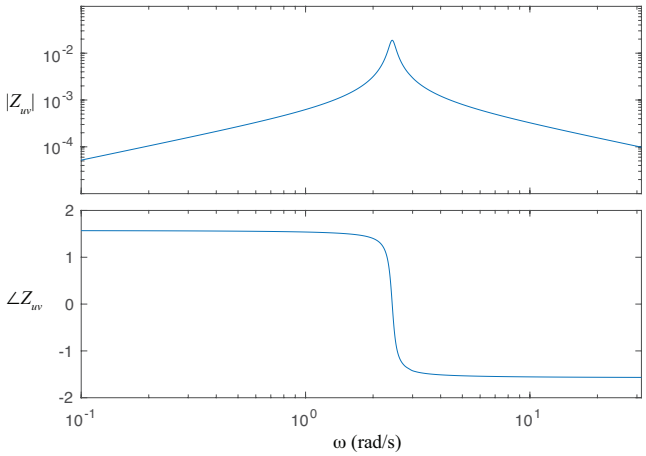

Fig. 6. Bode plot for Z_{uv} and Z_{fv}

implementation of this value may result in instability due to uncertainty in D_{uq} or T. As such, a value should be chosen which is the maximal value such that (99) can be assured, even in the presence of uncertainty.

V. Example

To demonstrate the control methodology described in the previous sections, we consider the small cylindrical buoy-type WEC shown in Figure 5. We assume the buoy is constrained to motion in heave. The mass of the buoy is 295kg, the diameter is 0.5m, and the draft is 1.5m. Bode plots for hydrodynamic transfer functions Z_{uv} and Z_{fv} are shown in Figure 6. (In this example, these two transfer functions are the same.)

We assume the maximum stroke of the bottom-mounted PTO is 1m. To model the PTO transmission losses, we assume a loss model as in (10), with $C = 1.5 \times 10^6$kg/s.

We assume the wave amplitude spectrum is a Pierson-Moskowitz spectrum [26] with a significant wave height of 1m, and a peak wave period of 9s.

We assume a sample time of $T = 0.1$s. For this case, Figure 7 shows the original infinite-dimensional discrete-time transfer function $H_{uq}(e^{j\Omega})$ (as derived in (18)), as well as its finite-dimensional approximation (as in (27)). Figure 8 shows the original infinite-dimensional discrete-time spectrum for $\Sigma_{wq}(j\Omega)$ (as in (19)), as well as its finite-dimensional approximation (as in (20) and (28)). We note that the total dimension of the discrete-time state space used to model these dynamics was 18.

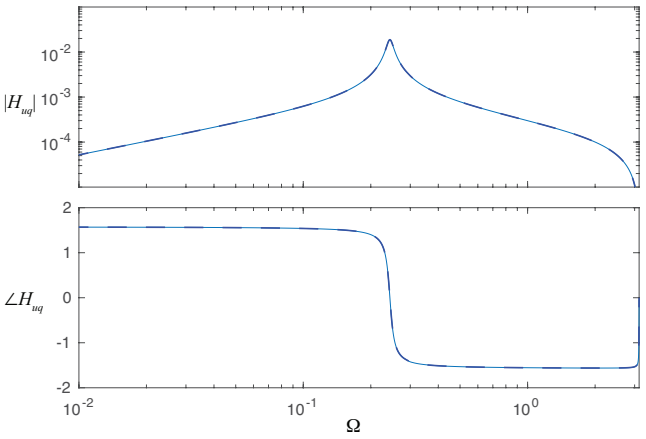

Fig. 7. Bode diagrams for infinite-dimensional H_{uq} (solid), as well as its finite-dimensional approximation (dash)

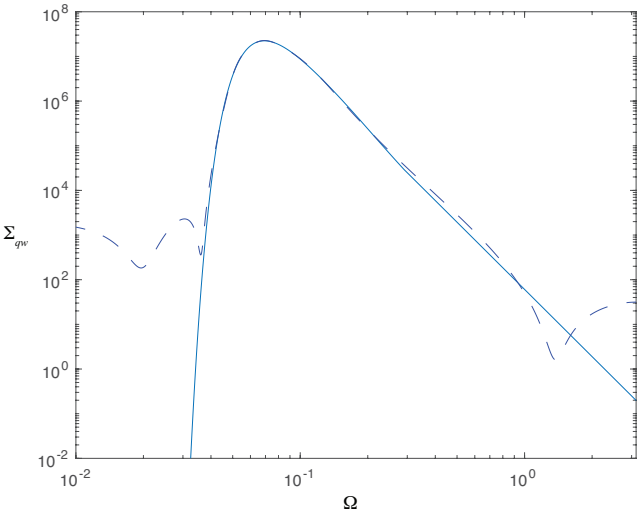

Fig. 8. Infinite-dimensional discrete-time force spectrum $\Sigma_{wq}(j\Omega)$ (solid), as well as the spectrum for its finite-dimensional approximation (dash)

For this case, the causal limit on the power that can be generated at this sample rate can be found via (56) to be 1490kW. However, this causal limit does not take the stroke limit into consideration, and is therefore considerably higher than the power that can be generated by the system under stroke constraints.

A. Performance of optimized linear controller

First we consider the linear control design described in Section III. In this case, we have an optimal linear performance (i.e., the maximized value of γ in optimization (75)) is 229kW. At this performance, the stroke covariance is equal to its constrained upper limit of $\frac{1}{4}d_m^2$. It is also interesting to note that the optimal linear feedback controller in this case is open-loop unstable.

Figure 9 shows transient plots for the stroke, force, and power, for one hour of data. Note that to achieve the optimal average power generation requires that the PTO be capable of bidirectional power flow. Also note that the relaxed stroke constraint has accomplished its desired goal, with the majority (but not all) of the displacement peaks occurring at displacements less than 1m.

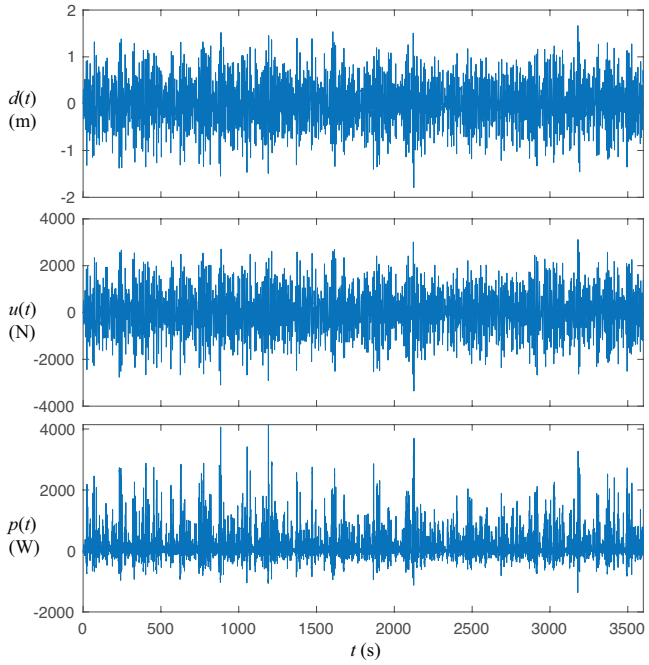

Fig. 9. Transient responses for linear control design with relaxed stroke constraint: PTO displacement d (top), PTO force u (middle), and generated power p (bottom)

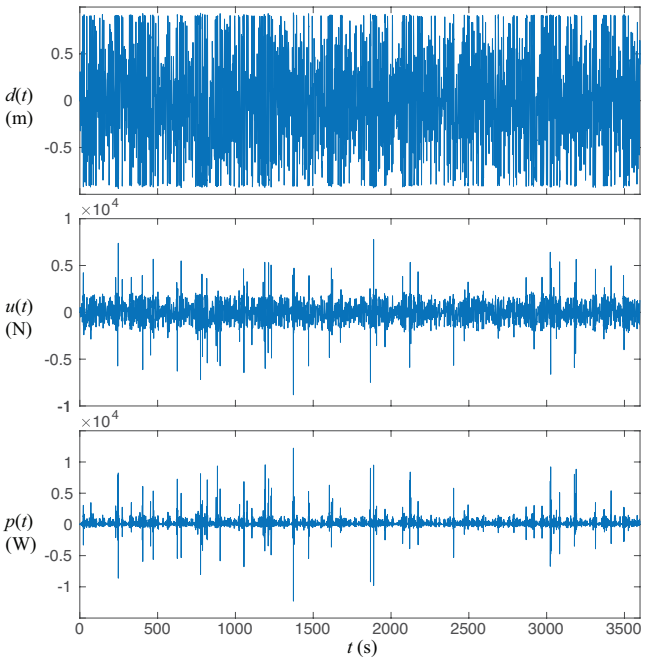

Fig. 10. Transient responses for linear control design with nonlinear stroke protection, with $\tau = 0$: PTO displacement d (top), PTO force u (middle), and generated power p (bottom)

B. Performance of nonlinear controller

To design the nonlinear controller, we take the parameter β (which determines the size of the safe zone in Figure 3 to be 0.9. To begin with, we consider the case in which the the nonlinear feedback law is chosen as in (90) with δ_k determined as in (86); i.e., we set the generalized parameter $\tau = 0$. We also presume Γ to be chosen as in (91).

For this scenario, Figure 10 shows the PTO displacement, force, and power for one hour of simulation time. As shown, the maximum stroke is maintained at $d_m = 1$m. Performance in this case is degraded somewhat, relative to the linear control design, with an average power generation of 204kW. However, we note that this amounts to only a 10% reduction in performance, which may be viewed as an acceptable compromise for stroke protection. Also note that, in order to protect the stroke, the controller applies very high PTO forces (and, consequently, high absorptive power levels) during periods when the stroke approaches its maximum allowable value.

It may be that in practice, the extremely high PTO forces in Figure 10 are impractical for a realistic system. In this case, the impulsive nature of the control force can be ameliorated by increasing the value of τ to something well above zero. To illustrate this, consider Figure 11, which shows transient responses for τ values of T, $10T$, and $100T$. We see that clearly, even with $\tau = 10T$, the impulses are virtually eliminated, while still providing (even more cautious) protection of the stroke. The tradeoff here is that by increasing τ one also must accept lower power generation performance. Specifically, the mean power generated for the three cases in the figure are 209, 187, and 45.4 kW, respectively.

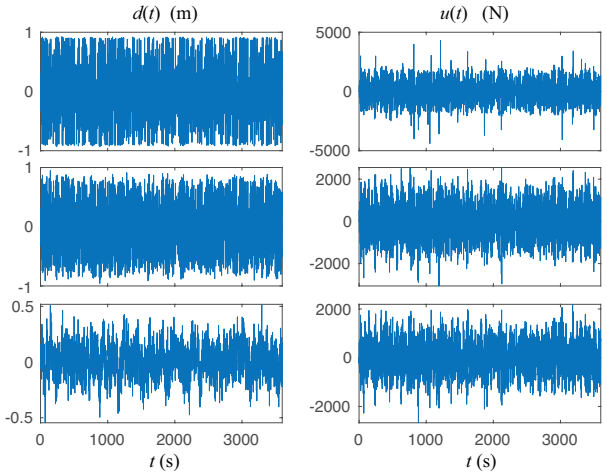

Fig. 11. PTO displacement (left) and force (right) trajectories for τ values of T (top), $10T$ (middle), and $100T$.

VI. Conclusions

The technique illustrated in this paper may be of value in the design of feedback controllers for WECs in which stroke saturation is a defining feature. The primary contribution of the paper has been to illustrate the manner in which the technique can be applied to discrete-time control systems, using a one-step-ahead predictor in conjunction with a nonlinear feedback law. Although the technique was demonstrated on a simple heaving buoy, the mathematical generality in which the ideas have been presented may make the technique applicable in many more WEC applications.

References

[1] S. H. Salter, "Wave power," *Nature*, vol. 249, pp. 720–724, 1974.
[2] K. Budal and J. Falnes, "A resonant point absorber for ocean wave power," *Nature*, vol. 257, pp. 478–479, 1975.

[3] D. V. Evans, "A theory for wave power absorption by oscillating bodies," *Journal of Fluid Mechanics*, vol. 77, pp. 1–25, 1976.
[4] ——, "Power from water waves," *Annual Review of Fluid Mechanics*, vol. 13, pp. 157–187, 1981.
[5] J. Falnes, "Radiation impedance matrix and optimum power absorption for interacting oscillators in surface waves," *Applied Ocean Research*, vol. 2, pp. 75–80, 1980.
[6] ——, *Ocean Waves and Oscillating Systems, Linear Interaction including Wave Energy Extraction*. Cambridge, UK: Cambridge University Press, 2002.
[7] S. H. Salter, J. R. M. Taylor, and N. J. Caldwell, "Power conversion mechanisms for wave energy," *Proceedings of the IME, Part M: Journal of Engineering for the Maritime Environment*, vol. 216, pp. 1–27, 2002.
[8] A. von Jouanne, "Harvesting the waves," *Mechanical Engineering*, vol. 128, pp. 24–27, 2006.
[9] A. Falcao, "Wave energy utilization: A review of the technologies," *Renewable and Sustainable Energy Reviews*, vol. 14, pp. 899–918, 2010.
[10] J. V. Ringwood, G. Baceli, and F. Fusco, "Energy-maximizing control of wave-energy converters: the development of control system technology to optimize their operation," *IEEE Control Systems Magazine*, vol. 34, pp. 30–55, 2014.
[11] J. J. Cândido and P. A. P. S. Justino, "Modelling, control and pontryagin maximum principle for a two-body wave energy device," *Renewable Energy*, vol. 36, pp. 1545–1557, 2011.
[12] J. A. M. Cretel, G. Lightbody, G. P. Thomas, and A. W. Lewis, "Maximisation of energy capture by a wave-energy point absorber using model predictive control," in *Proceedings, IFAC World Congress on Automatic Control*, Milano, Italy, 2011.
[13] J. Hals, J. Falnes, and T. Moan, "Constrained optimal control of a heaving buoy wave-energy converter," *Journal of Offshore Mechanics and Arctic Engineering*, vol. 133, 2011, # 011401.
[14] M. Richter, M. E. Magaña, O. Sawodny, and T. K. Brekken, "Nonlinear model predictive control of a point absorber wave energy converter," *Sustainable Energy, IEEE Transactions on*, vol. 4, no. 1, pp. 118–126, 2013.
[15] E. Abraham and E. C. Kerrigan, "Optimal active control and optimization of a wave energy converter," *IEEE Transactions on Sustainable Energy*, 2012, (in press).
[16] J. T. Scruggs, S. M. Lattanzio, A. A. Taflanidis, and I. L. Cassidy, "Optimal causal control of a wave energy converter in a random sea," *Applied Ocean Research*, vol. 42, pp. 1–15, 2013.
[17] J. T. Scruggs, "Causal control design for wave energy converters with finite stroke," in *Proceedings, IFAC World Congress on Automatic Control*, Toulouse, France, 2017.
[18] J. T. Scruggs, Y. Lao, A. Karthikeyan, and M. Previsic, "A new passivity-based nonlinear causal control technique for wave energy converters with finite stroke," in *Proceedings, American Control Conference*, Philadelphia, USA, 2019.
[19] B. D. O. Anderson and S. Vongpanitlerd, *Network Analysis and Synthesis: A Modern Systems Theory Approach*. Englewood Cliffs, NJ: Prentice-Hall, 1973.
[20] J. Scruggs and R. Nie, "Disturbance-adaptive stochastic optimal control of energy harvesters, with application to ocean wave energy conversion," *Annual Reviews in Control*, vol. 40, pp. 102–115, 2015.
[21] H. Akcay, "Frequency domain subspace-based identification of discrete-time power spectra from uniformly spaced measurements," *Automatica*, vol. 47, no. 2, pp. 363–367, 2011.
[22] J. T. Scruggs, "On the causal power generation limit for a vibratory energy harvester in broadband stochastic response," *Journal of Intelligent Material Systems and Structures*, vol. 21, pp. 1249–1262, 2010.
[23] C. Scherer, P. Gahinet, and M. Chilali, "Multiobjective output-feedback control via lmi optimization," *IEEE Transactions on automatic control*, vol. 42, no. 7, pp. 896–911, 1997.
[24] C. A. Desoer and M. Vidyasagar, *Feedback systems: input-output properties*. Siam, 2009, vol. 55.
[25] R. Lozano, B. Brogliato, O. Egeland, and B. Maschke, *Dissapative Systems Analysis and Control*, 2nd ed. London: Springer-Verlag, 2007.
[26] O. M. Faltinsen, *Sea Loads on Ships and Offshore Structures*. Cambridge University Press, 1990.